

Compact MEMS-SPICE Modeling

Hoan H. Pham and Arokia Nathan

Electrical and Computer Engineering, University of Waterloo
Waterloo, Ontario N2L 3G1, Canada

(Received October 9, 1997; accepted January 20, 1998)

Key words: mixed-signal simulation, multivariate-polynomial-dependent sources, electrostatic pull-in, constant-charge operation

We present a technique using multivariate-dependent sources that enables synthesis of simple and compact circuit models, and which is effective in handling mixed signal coupling and its intrinsic nonlinearity. Models are presented for electrothermal and electromechanical microsystems, along with SPICE simulation examples of vertical and torsional electrostatic microactuators under constant-voltage and constant-charge operating modes, and their effect on electrostatic pull-in.

1. Introduction

The microtransducer in mixed-signal microsystems is central to the control and feedback operation and hence, cannot be isolated from the circuitry in the design process. Here, the model or tool must account for device-circuit interactions as well as provide reasonably accurate functional descriptions for both. Device-circuit interactions can be handled either in a device or circuit simulation environment. We adopt the latter environment. Using suitable isomorphisms between mixed-signal physical variables, we report a technique for the synthesis of compact circuit models, using multivariate-polynomial-dependent sources that are compatible with standard circuit simulators such as SPICE. We choose SPICE because it is the current industry standard.

Interactions between mixed signals may be strongly coupled. In many cases, the coupling can be highly nonlinear. Mixed-signal coupling has been treated using several approaches including analog computer techniques,⁽¹⁾ direct synthesis from numerical simulators,⁽²⁾ domain decoupling,⁽³⁾ and dependent passive elements. In this letter, we summarize the last of these approaches, the results for which were first presented at the

CAD for MEMS workshop;⁽⁴⁾ a comprehensive version of the work will be presented in the Special Issue on CAD for MEMS.⁽⁵⁾ The approach stems from bond graph theory⁽⁶⁾ whereby coupling elements can be described in terms of passive elements such as dependent resistors (R), dependent capacitors (C), or dependent inductors (L). However, the resulting circuit can have different equivalent forms and care is needed to identify the most appropriate form in terms of simplicity, effectiveness, and comprehensibility to allow insight into system behavior under different geometric and operating conditions.

2. Multivariate-Polynomial-Dependent Sources

Most mixed-signal systems have passive elements (*e.g.*, R , C , L) which are dependent on some variable excitation or detection signal (x), and serve as a source of coupling. Since not all circuit simulators support passive elements whose values change during the course of simulation, we must find an alternate means of expressing this dependence. Fortunately, multivariate-polynomial-dependent sources have become a standard feature in state-of-the-art SPICE-like simulators.

We denote a dependent passive element, $P \in \{R, C, L\}$, whose value $P(x)$ is dependent on some signal x such as temperature or mechanical displacement, *viz.*,

$$P(x) = P_0 [1 + f(x)] \quad (1)$$

$$\frac{1}{P(x)} = \frac{1}{P_0} [1 + g(x)], \quad (2)$$

where $f(x)$ and $g(x)$ are polynomial functions of the external signal x and P_0 is the unperturbed ($x = 0$) value of the element. We decompose either $P(x)$ or $1/P(x)$ into two components, one which is independent of x and the other which can be realized using a polynomial-dependent source. Either eq. (1) or (2) will suffice in describing the coupling element; the choice depends on the behavior of the physical system. If there is a tendency for $P(x)$ to become large, then the choice lies in eq. (2).

3. The Dependent Resistor

In this case, $P(x)$ denotes a resistor, $R \equiv R(x)$. With eq. (1), we choose the constitutive relation $V = iR(x)$. This yields, following (1),

$$iR_0 [1 + f(x)] = iR_0 + iR_0 f(x), \quad (3)$$

where we have an independent resistor R_0 whose voltage drop is V_0 . Thus $V = V_0 + V_0 f(x)$ where the dependence of R on x can now be described by an independent resistor R_0 and a dependent voltage-controlled voltage source (VCVS) whose value is $V_0 f(x)$. The circuit realization is depicted in Fig. 1.

In the case of the polynomial equation (2), we choose the constitutive relation, $i = V/R(x)$. This yields, following (2),

$$i = \frac{V[1 + g(x)]}{R_0} \tag{4}$$

Here, i is the current through $R(x)$ and V is the associated voltage drop. This current can also be viewed as the current through the resistor R_0 , the voltage across which is $V[1 + g(x)]$. Thus we can connect an independent resistor R_0 and a VCVS of value $-Vg(x)$ in series. The circuit realization is depicted in Fig. 2.

We apply the above synthesis scheme to an electrothermal system where coupling stems from the temperature dependence of electrical resistance and Joule heat. For small variations in temperature T , the electrical resistance R can be modeled in terms of its temperature coefficient α , viz., $R(T) = R_0 [1 + \alpha T]$, which yields an exact polynomial of eq.

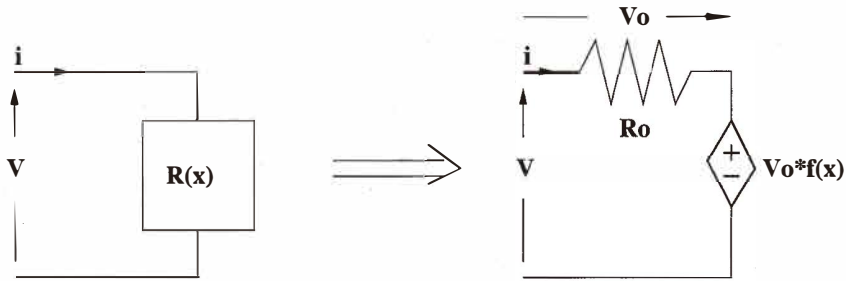


Fig. 1. Dependent source realization of coupling resistor, $R(x) = R_0[1 + f(x)]$.

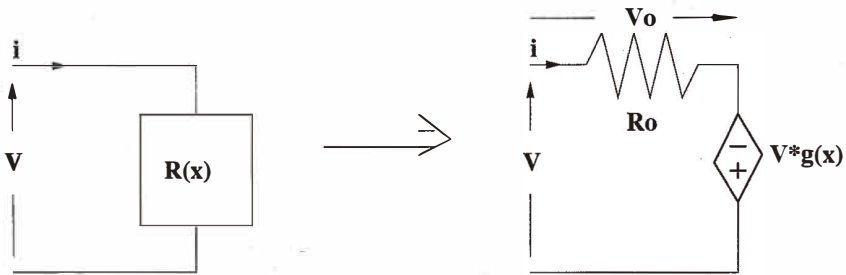


Fig. 2. As in Fig. 1, but for coupling resistor, $\frac{1}{R(x)} = \frac{1}{R_0}[1 + g(x)]$.

(1). For an isothermal resistor with heat transfer to the environment (T_∞) described by a heat transfer coefficient (h), the model equations for the electrothermal system can be reduced (see ref. 5).

$$V = V_{12} + V_{12} \alpha T \tag{5}$$

$$V \frac{V_{12}}{R_o} = C \frac{dT}{dt} + h(T - T_\infty) \tag{6}$$

whose equivalent circuit is given in Fig. 3. Here, the voltage V_3 represents temperature, V denotes the voltage across the electrothermal resistor, C the thermal capacitance, V_{12} the voltage across the resistor R_o (across nodes 1 and 2), and the bivariate polynomial VCVS of value VV_{12}/R_o represents Joule heat. The circuit in Fig. 3 can be employed to simulate transient electrothermal behavior.

4. The Dependent Capacitor

In this case, $P(x)$ in eqs. (1) and (2) denotes a capacitor $C \equiv C(x)$. By replacing i with q and R_o with $1/C_o$, we can identify the correspondence between the resistor and capacitor: ($V = iR$) \leftrightarrow ($V = q/C$). With polynomial equation (1), we obtain

$$q = CV = C_o [1 + f(x)] V, \tag{7}$$

where q is the charge on the plate of the capacitor C_o , the voltage across which is $V[1 + f(x)]$. This is analogous to the case of the dependent resistor associated with the polynomial equation (2). A realization of $C(x)$ is shown in Fig. 4. The circuit is similar in structure to the one shown in Fig. 2.

In the case of the polynomial equation (2), by choosing the constitutive relation $V = q/$

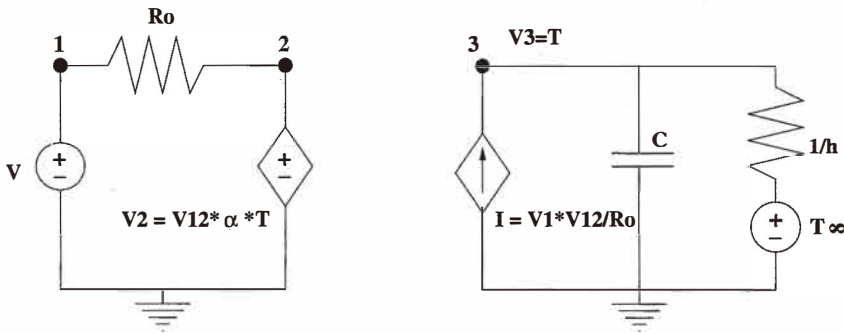


Fig. 3. Equivalent circuit for electrothermal resistor, $R(T)$.

C, we obtain

$$V = \frac{q}{C_0} [1 + g(x)] = V_0 + V_0 g(x), \tag{8}$$

where $V_0 = (q/C_0)$. The voltage V across the dependent capacitor C can be viewed as a sum of two voltages: the voltage V_0 of the independent C_0 and the VCVS of value $V_0 g(x)$. A realization of $C(x)$ in this case is shown in Fig. 5. The circuit has a structure similar to that shown in Fig. 1.

Using the above synthesis scheme, we simulate an electrostatically actuated parallel plate capacitor whereby the coupling stems from the dependence of capacitance on mechanical displacement. In bond graph terminology, the actuator is a two-port C-field. In modeling the electromechanical system, the constitutive relationship between the variables force (F), displacement (x), plate voltage (V_p), and charge (q), is constructed by expressing C in terms of x , and F in terms of V_p and x . The model equations for electrical and

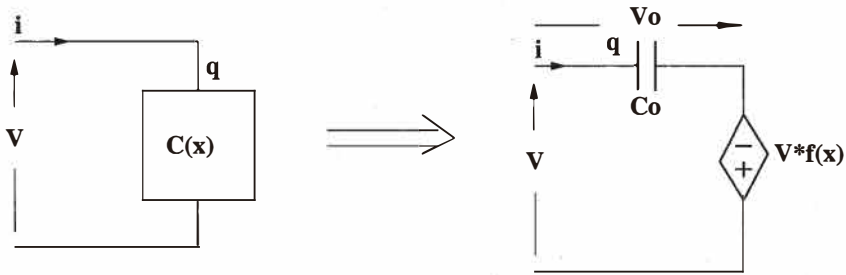


Fig. 4. Dependent source realization of coupling capacitor, $C(x) = C_0 [1 + f(x)]$.

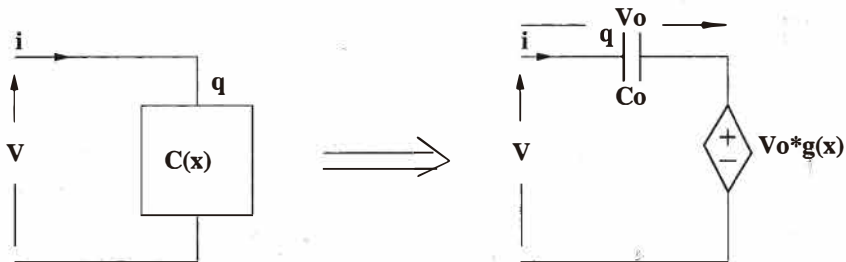


Fig. 5. As in Fig. 4, but for coupling capacitor, $\frac{1}{C(x)} = \frac{1}{C_0} [1 + g(x)]$.

mechanical operation are

$$V_p = V_{in} - iR \text{ with } i = dq/dt \quad (9)$$

$$F = m \frac{d^2x}{dt^2} + b \frac{dx}{dt} + kx \quad (10)$$

with the usual notation (see ref. 7). The capacitance C can be expressed as

$$C = \frac{\epsilon A}{d-x} = \frac{\epsilon A}{d} \frac{d}{d-x} = C_0 \frac{d}{d-x}, \quad (11)$$

where C_0 denotes the initial capacitance (when $x=0$), d the initial distance between the two plates, ϵ the permittivity of the associated dielectric (assumed to be air), and A the plate area. For the electrostatic force F , we employ

$$F = \frac{\epsilon A}{2(d-x)^2} V_p^2. \quad (12)$$

Thus the complete electromechanical system is modeled using eqs. (9) to (12).

The difficulty with the above equation stems from the high nonlinearity associated with the plate displacement, which requires the use of a time-varying capacitor model,⁽⁷⁾ small signal approximation,⁽⁸⁾ or Taylor expansion,⁽⁹⁾ since

$$\lim_{x \rightarrow d} C = \lim_{x \rightarrow d} \epsilon A / (d-x) = \infty. \quad (13)$$

This limitation can be overcome by employing an alternate form of the constitutive relation, viz.,

$$\frac{1}{C} = \frac{1}{C_0} \left(1 - \frac{x}{d} \right), \quad (14)$$

which is of the form given by eq. (2) whereby $g(x) \equiv -x/d$. Thus, although C does not have an exact polynomial form, see eq. (11), $1/C$ as described by eq. (14) does, allowing use of a multivariate-polynomial-dependent source. Furthermore, by replacing V_p in eq. (12) with $V_p = q/C$, we can express the electrostatic force in terms of charge using

$$F = \frac{q^2}{C_0 d}. \quad (15)$$

Equation (15), in terms of charge, constitutes a more convenient form, compared to eq. (12), for dealing with nonlinearity.

Equation (14) for the capacitance can be realized using the circuit shown in Fig. 4. If V_{23} (instead of V_0) denotes the voltage across C_0 , the charge, $q = \int i dt$ on the dependent capacitor C , is also the charge q on the independent capacitor C_0 . Therefore,

$$q = C_0 V_{23}. \quad (16)$$

The voltage across the dependent capacitor and the force, given by eq. (15), become

$$V_p = V_{23} - V_{23} \frac{x}{d} \quad (17)$$

$$F = \frac{C_0}{2d} V_{23}^2. \quad (18)$$

Thanks to the inclusion of capacitor C_0 , we have also managed to eliminate the need to integrate dq/dt . In fact, q is eliminated and replaced by $C_0 V_{23}$, as given by eq. (16). Equation (18) suggests the realization of force using a polynomial VCVS of value $(C_0/2d) V_{23}^2$. The next step lies in obtaining the displacement x without the use of an integrator. Employing an alternate set of analogies (see Table 1), we can model the mechanical operation, eq. (10), using a VCVS and a serial RLC circuit in which kx is the voltage across the capacitor whose capacitance is $1/k$. Denoting this voltage by V_6 , we obtain $x = V_6/k$, and eq. (17) becomes

Table 1

Alternate set of analogies between electrical and mechanical domains for synthesis of electromechanical equivalent circuits.

Electrical	Translational mechanics
voltage V	force F
charge q	displacement x
current i	velocity $v = dx/dt$
di/dt	acceleration dv/dt

$$V_p = V_{23} - V_{23} \frac{V_6}{kd}. \quad (19)$$

The model equations for the complete electromechanical system now become eqs. (9), (10), (18) and (19). Figure 6 shows the resulting equivalent circuit for the electromechanical system. Here, the voltage V_4 represents the electrostatic force F , and V_2 denotes the plate voltage V_p . SPICE simulation results of displacement as a function of plate voltage are shown in Fig. 7 for constant-voltage and constant-charge operation modes. Relevant data for the simulations are extracted from ref. 10. Under constant voltage, electrostatic pull-in occurs when x approaches $d/3$. Under constant-charge operation, however, the plate can be displaced in a controlled manner between 0 and d .

5. SPICE Simulation of Electrostatic Micromirror

Using the above synthesis technique, we now illustrate the SPICE simulation of a CMOS electrostatic micromirror.⁽¹¹⁾ Figure 8 shows a schematic of the mirror used in the analysis. The mirror consists of a rotating plate RP, two fixed electrode plates EP1 and EP2, and two landing plates LP1 and LP2. The rotating plate RP has a length $2l_0$, rotates about the pivot in the center, and is grounded. The fixed electrodes EP1 and EP2 have length l , with $l < l_0/2$. When one of the electrodes is biased, RP rotates under the action of the electrostatic force. If the bias voltage is large enough, electrostatic pull-in occurs and RP comes in contact with the closest LP.

Equivalent circuit modeling of the micromirror is similar to the vertically actuated parallel plate capacitor, except that we now have rotational movement (see comparison of associated variables in Table 2). There are three dominant mutual capacitors C_{01} , C_{02} , and C_{12} for the pairs of plates (RP, EP1), (RP, EP2), and (EP1, EP2), respectively. Due to symmetry, $C_{01} = C_{02}$. Furthermore, we can safely assume that $C_{12} \ll C_{01}$; hence, we ignore the contribution of C_{12} . The capacitor, C_{01} or C_{02} , can be approximated as⁽⁵⁾

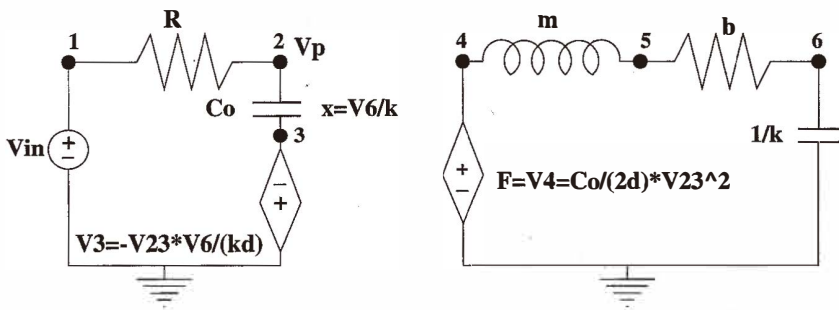


Fig. 6. Equivalent circuit for electromechanical capacitor.

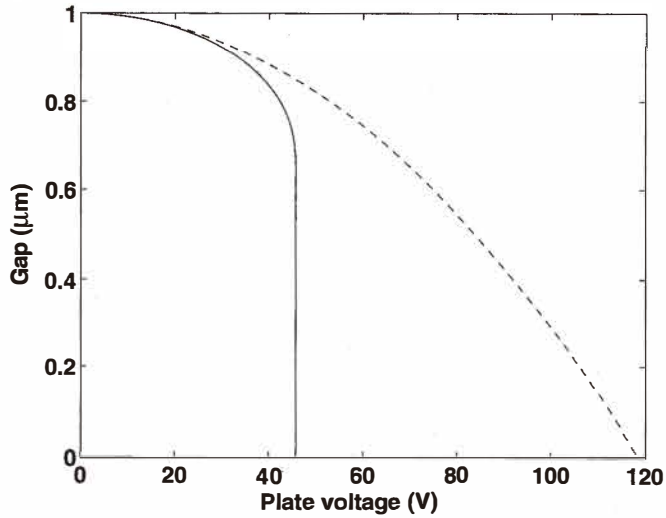


Fig. 7. SPICE simulation of displacement under constant-voltage (solid curve) and constant-charge (dashed curve) operation modes for a parallel plate actuator.

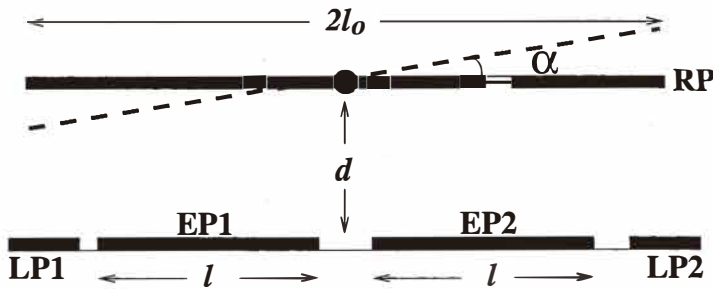


Fig. 8. Schematic for electrostatic micromirror used in SPICE simulations.

$$C \approx C_0 \frac{\ln(1+x)}{x}, \tag{20}$$

where $C_0 = \epsilon W l d$ denotes the capacitance when the rotation angle $\alpha = 0$ and $x = -(l/d)\alpha$. Equation (20), in its given form, is not suitable for simulation since it has an indeterminate form at $x = 0$. Using Taylor's series, we expand either $(1/x) \ln(1+x)$ or $x/\ln(1+x)$. The latter is preferable since it approaches 0 when x approaches -1 . Hence,

Table 2
List of duals for translational and rotational mechanics.

Translational mechanics	Rotational mechanics
force F	torque τ
displacement x	rotation angle α
mass m	moment of inertia I
spring constant k	torsion constant κ
damper b	damper b

$$\frac{1}{C} \approx \frac{1}{C_0} g(x), \text{ with } g(x) = \begin{cases} \frac{x}{\ln(1+x)} \\ 1 + \frac{1}{2}x - \frac{1}{12}x^2 + \frac{1}{24}x^3 - \frac{19}{720}x^4 + \dots O(x^{n+1}), \end{cases} \quad (21)$$

and the respective model equations for the torque τ are

$$\tau = \frac{1}{2} V^2 \frac{dC}{d\alpha} \approx \begin{cases} \frac{1}{2C_0} \frac{1}{d} q^2 g'(x) & \text{constant charge} \\ \frac{1}{2} C_0 \frac{1}{d} V^2 \frac{g'(x)}{g^2(x)} & \text{constant voltage.} \end{cases} \quad (22)$$

The above approximate models for the capacitance C and torque τ have been verified using numerical simulation based on the panel method (see ref. 5). The relations used in the simulation of the coupled electromechanical circuit (Fig. 6) are summarized in Table 3. The circuit model yields good agreement with numerically obtained values.⁽¹¹⁾ The torsion constant κ needed in the SPICE simulations is extracted from measured data⁽¹¹⁾ of the critical (pull-in) voltage V_c , which is taken to be 12.5 V.

To determine the critical angle and critical voltage at electrostatic pull-in, we solve for α using the following system of equations:

$$\tau(\alpha) = \kappa\alpha, \quad \frac{\partial\tau(\alpha)}{\partial\alpha} = \kappa, \tag{23}$$

where τ is given in Table 3. A summary of the results is given in Table 4 for the two modes. Based on these results, we now analyze the electrostatic pull-in behavior.

Unlike the vertically actuated parallel plate capacitor where constant charge operation eliminates electrostatic pull-in, the micromirror is subject to pull-in even under constant-charge operation, since the torque is not constant despite a constant-charge operation. This is due to the nonconstant term $g'(x)$ in eq. (22). However, the relations in Table 4 suggest that for a given geometry (l_0 , l and d), the onset of electrostatic pull-in could be delayed. Figure 9 shows the angle of rotation as a function of applied bias under constant-charge and constant-voltage operation modes. As predicted (see Table 4), the critical angle under constant-charge operation is larger than that under constant-voltage operation. Also, by changing the micromirror geometry, we can delay the onset of pull-in, even under constant-voltage operation. For both operation modes, this can be achieved by choosing l small enough so that the relative angle, r_q or r_v , becomes unity. Figure 10 shows how the relative

Table 3

Summary of model equations for capacitance and torque (under constant-charge operation) used in micromirror simulations.

Capacitance	$\frac{1}{C(\alpha)} = \frac{1}{C_0} \left[1 - \frac{1}{2} \frac{1}{d} \alpha - \frac{1}{12} \left(\frac{1}{d} \right)^2 \alpha^2 - 2 \frac{1}{24} \left(\frac{1}{d} \right)^3 \alpha^3 \right]$
Torque	$\tau(\alpha) = \frac{1}{2C_0} \frac{1}{d} q^2 \left[\frac{1}{2} + \frac{1}{6} \frac{1}{d} \alpha + \frac{1}{8} \left(\frac{1}{d} \right)^2 \alpha^2 + \dots + 2 \frac{33953}{453600} \left(\frac{1}{d} \right)^7 \alpha^7 \right]$

Table 4

Summary of results of electrostatic pull-in associated with constant-voltage and constant-charge operation modes of micromirror.

Operation mode	Critical angle	Relative angle	Critical voltage
Constant charge	$\alpha_q = 0.71 \frac{d}{l}$	$r_q = \frac{\alpha_q}{\alpha_{max}} = 0.71 \frac{l_0}{l}$	$V_{C,q} = 1.34 \frac{d}{l} \sqrt{\frac{\kappa}{C_0}}$
Constant voltage	$\alpha_v = 0.44 \frac{d}{l}$	$r_v = \frac{\alpha_v}{\alpha_{max}} = 0.44 \frac{l_0}{l}$	$V_{C,v} = 0.91 \frac{d}{l} \sqrt{\frac{\kappa}{C_0}}$

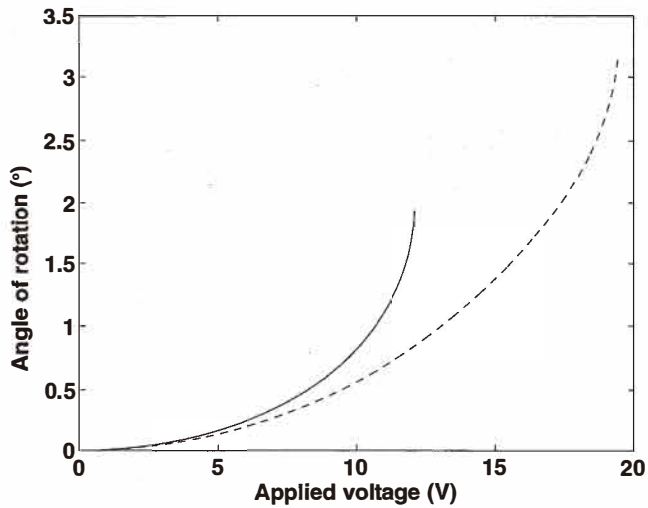


Fig. 9. A comparison of rotation behavior associated with electrostatic pull-in under constant-voltage (solid curve) and constant-charge (dashed curve) operation modes.

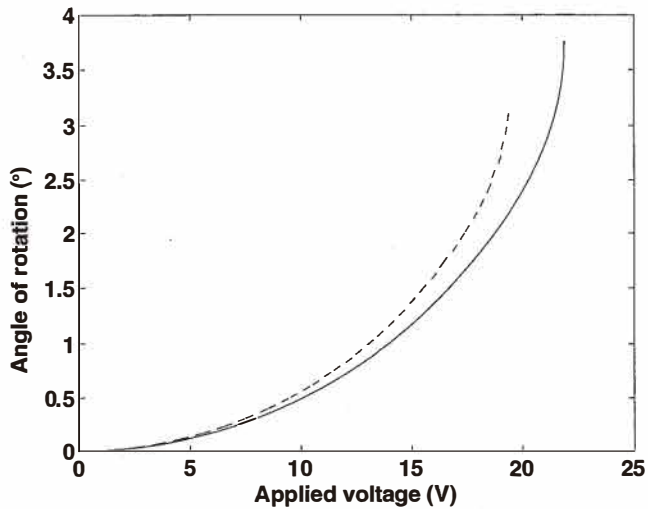


Fig. 10. A comparison of rotation behavior under constant-charge operation for different micromirror electrode geometries: $l_0/l = 20 \mu\text{m}/16 \mu\text{m}$ (solid curve) and $l_0/l = 20 \mu\text{m}/18 \mu\text{m}$ (dashed curve).

angle can be improved by increasing the ratio l_0/l . However, a smaller value of l or a larger value of d decreases the initial capacitance C_0 , and results in an increase in the applied voltage required to achieve the same angle of rotation.

6. Conclusions

Mixed-signal simulation using circuit simulators can provide a low-cost and expedient means of designing microsystems. The challenge lies in the synthesis of reliable equivalent circuit models that can effectively accommodate mixed signal coupling and associated intrinsic nonlinearity. The technique presented here exploits multivariate-dependent passive sources to describe the nonlinear coupling behavior, and has been demonstrated to be very effective for the synthesis of compact mixed-signal circuit models that are compatible with standard circuit simulators such as SPICE.

References

- 1 N. M. Karaynakis: Computer-Assisted Simulation of Dynamic Systems with Block Diagram Languages (CRC Press, Florida, 1993).
- 2 J. G. Korvink, M. Bächtold, M. Emmenegger, R. Paganini, R. Ruehl, J. Funk and H. Baltes: Proc. ESSDERC '96, eds. G. Baccarani and M. Rudan (1996) p. A5.
- 3 N. R. Swart and A. Nathan: Sensors and Materials **6** (1994) 179.
- 4 CAD for MEMS Workshop 1997 (Zürich, 1997).
- 5 H. Pham and A. Nathan: "Circuit modeling and SPICE simulation of mixed-signal microsystems," Sensors and Materials, Special Issue on CAD for MEMS, to appear.
- 6 D. Karnopp, D. Margolis and R. Rosenberg: System Dynamics: A Unified Approach (John Wiley, New York, 1990) 2nd ed.
- 7 G. K. Fedder and R. T. Howe: IEEE J. of MEMS **5** (1996) 283.
- 8 H. A. C. Tilmans: J. Micromech. Microeng. **6** (1996) 157.
- 9 S. D. Senturia: Digest of Technical Papers, Transducers'95 (Stockholm 1997) p. 5.
- 10 P. Osterberg, H. Yie, X. Cai, J. White and S. D. Senturia: IEEE MEMS Workshop 1994 (IEEE 1994) p. 28.
- 11 J. Funk, J. G. Korvink, M. Bächtold, J. Bühler and H. Baltes: IEEE MEMS Workshop 1996 (IEEE 1996) p. 133.